Geomechanics and Engineering, *Vol. 31, No. 5 (2022) 529-543*
https://doi.org/10.12989/gae.2022.31.5.529

Lattice-spring-based synthetic rock mass model calibration using response surface methodology

Mariam Al-E'Bayat[1], Taghi Sherizadeh*[2], Dogukan Guner[2] and Mostafa Asadizadeh[2]

[1]*Department of Geosciences and Geological and Petroleum Engineering, Missouri University of Science and Technology, Rolla, MO 65409, USA*
[2]*Department of Mining and Explosives Engineering, Missouri University of Science and Technology, Rolla, MO 65409, USA*

(*Received November 28, 2021, Revised November 20, 2022, Accepted December 7, 2022*)

Abstract. The lattice-spring-based synthetic rock mass model (LS-SRM) technique has been extensively employed in large open-pit mining and underground projects in the last decade. Since the LS-SRM requires a complex and time-consuming calibration process, a robust approach was developed using the Response Surface Methodology (RSM) to optimize the calibration procedure. For this purpose, numerical models were designed using the Box–Behnken Design technique, and numerical simulations were performed under uniaxial and triaxial stress states. The model input parameters represented the models' micro-mechanical (lattice) properties and the macro-scale properties, including uniaxial compressive strength (UCS), elastic modulus, cohesion, and friction angle constitute the output parameters of the model. The results from RSM models indicate that the lattice UCS and lattice friction angle are the most influential parameters on the macro-scale UCS of the specimen. Moreover, lattice UCS and elastic modulus mainly control macro-scale cohesion. Lattice friction angle (flat joint fiction angle) and lattice elastic modulus affect the macro-scale friction angle. Model validation was performed using physical laboratory experiment results, ranging from weak to hard rock. The results indicated that the RSM model could be employed to calibrate LS-SRM numerical models without a trial-and-error process.

Keywords: lattice-spring-based synthetic rock mass; LS-SRM model; response surface method; SRMTools

1. Introduction

The estimation of strength and deformability characteristics of rock mass is still a challenging issue. The rock mass response is governed by the mechanical characteristics of the intact rock, the density of discontinuities, and their orientations (Oge 2020). These parameters are usually evaluated using laboratory and field tests that are time-consuming, complicated, and impractical to perform on large-scale specimens physically. Conversely, the numerical modeling approach is flexible, low cost, can provide reproducible results, and can easily be employed to simulate rock volumes of any size (Jing 2003, Oge 2021). In the last decades, numerical methods have been extensively used to determine the mechanical properties of rock mass (Di *et al*. 2011, Farahmand *et al*. 2018, Liu *et al*. 2018, Meng *et al*. 2019, Wang and Yan 2020).

Numerical modeling approaches can be classified into continuum, discontinuum, and hybrid techniques. Continuum techniques include the Boundary Element Method (BEM), Finite Element Method (FEM), and Finite Difference Method (FDM), which are suitable for modeling jointed rocks with a homogeneous distribution of discontinuities. Discontinuum techniques such as the Distinct Element Method (DEM) (Cundall 1971) and the Discontinuous Deformation Analysis (DDA) (Gen-Hua and Shi 1989) are widely used for simulating jointed rock mass, as failure in both the intact rock mass and along pre-existing discontinuities are taken into account (Huang *et al*. 2015, Li *et al.* 2018, Sarfarazi *et al*. 2016, Scholtès and Donzé 2015, Zhou and Chen 2019, Xu *et al.* 2020). The hybrid technique combines continuum and discontinuum methods applicable to model large-scale jointed rock mass. A hybrid technique, like FEM-DEM, has been used to evaluate the stability of a mine pillar (Elmo and Stead 2010) and simulate the fracture-fragmentation of geologic materials (Morris *et al*. 2006). Eberhardt *et al*. (2003) utilized a hybrid method to replicate the step path failure in massive rock slopes. Barla *et al*. (2012) employed the same technique to analyze the rockslide failure at the Alpetto Mine in Italy. In rock mass modeling, DEM considers the progress of failure partly through the intact rock and partly along pre-existing discontinuities. Moreover, the DEM approach can simulate complex failure mechanisms, such as fracture opening, sliding, and the propagation of microcracks in brittle rocks (Camones *et al.* 2013a).

Synthetic Rock Mass (SRM) and the SRM approach was developed in the mass mining technology project to describe the discontinuum numerical modeling and to quantify the mechanical properties of rock mass (Pierce *et al.* 2007). Although this approach was initially implemented with Particle Flow Code (PFC3D) using the bonded particle model (BPM) approach, it was later also employed in Universal Distinct Element Code (UDEC) based on bonded block model (BBM) technique (Itasca 2019).

*Corresponding author, Assistant Professor
E-mail: sherizadeh@mst.edu

ISSN: 2005-307X (Print), 2092-6219 (Online)

In BBM, the synthetic rock mass is represented by either rigid or deformable blocks, and the boundaries of the blocks represent the discontinuities. Although both BBM and BPM-based SRM approaches are computationally intensive, they were used to efficiently simulate the laboratory test of veined core samples (Turichshev and Hadjigeorgiou 2017, Vallejos *et al.* 2016). In addition, several authors utilized the BPM and BBM approach in rock slope stability research (Brideau *et al*. 2011, Camones *et al.* 2013, Havaej and Stead 2016).

Slope Model software, a recent code developed by Itasca Consulting Group, is also based on the SRM approach (Itasca 2016). The drawback of the high computational demand of the other SRM based approach is eliminated in this code by replacing the bonded particle/block with a lattice. Therefore, the approach used by this code is called lattice-spring-based synthetic rock mass modeling (LS-SRM).

The LS-SRM method has been employed in various slope stability projects in the last decade to quantify the brittle fracturing effect (Cundall *et al*. 2016, Havaej and Stead 2016, Herrero 2015, Poulsen *et al.* 2015). Bastola and Cai (2018a) adopted the LS-SRM approach to evaluate the macro mechanical parameters of rock and joints in Blanco Mera granite. This approach was also employed to simulate the crack mechanisms of jointed marble under unconfined and confined compression tests (Bastola and Cai 2019).

In all SRM approaches, proper selection of micro-scale or lattice parameters is required at the beginning of the model stage to simulate the exact responses of the rock mass. Generally, parameters obtained from laboratory experiments are used to derive these parameters. This calibration stage is based on a trial-and-error process in which high computational performance is needed to run the models. Although some attempts have been made to simplify the calibration process, only a few studies have focused on developing methods for parameter quantification. Therefore, statistical analysis methods were employed along with numerical approaches to generate models with random input variables from corresponding probabilistic distributions to determine the solution statistically.

The Monte Carlo simulation (MCS) technique was widely used in conjunction with numerical methods for evaluating the reliability of rock mass analysis. Rasmussen *et al*. (2019) applied a combination of a Lattice model and MCS to analyze rock tunnels in environments with low levels of in-situ stress. MCS and FEM were used to evaluate slope stability in variable soils (Griffiths and Fenton 2004, Huang *et al.* 2010, Li *et al*. 2014). However, the main drawback of MCS is the large number of model runs required to obtain representative results. Response Surface Methodology (RSM) is efficiently used as an alternative to MCS in slope reliability problems since it can minimize the required running models. Several researchers implemented the RSM technique in rock mechanics and calibration studies (Dadashzadeh *et al*. 2017, Jiang *et al.* 2014, Li *et al.* 2013, Li *et al.* 2011, Chehreghani *et al*. 2017). Moreover, the design of experiments (DOE) methods is also used to develop more efficient DEM calibration approaches. Yoon (2007) implemented a statistical central composite design (CCD) method for PFC to determine suitable DEM microparameters under a uniaxial stress state. Johnstone and Ooi (2010) used DOE methods to calibrate numerical models based on experimental measurements of triaxial compression tests.

This paper aims to quantify the relationships between micro and macro-scale rock properties for utilization in LS-SRM models and develop a novel statistical model capable of facilitating the calibration process. For this purpose, Box–Behnken Response Surface Methodology (RSM) was adopted to design experiments and optimize the input micro-properties (lattice parameters). After the required model numbers were determined by Box–Behnken methodology, the numerical modeling part of the study was started. A total of 29 LS-SRM model runs were conducted to obtain input parameters for multiple regression and response surface models. Then, statistical-mathematical models were proposed for the estimation of the rock mass parameters to aid further studies. The effect of each variable and their mutual contributions were then evaluated using four response surface models. Finally, the proposed models were validated with five rock types, from weak to strong. The flowchart diagram of the model calibration procedure is presented in Fig. 1.

2. Lattice-spring-based synthetic rock mass (LS-SRM) modeling approach

In lattice-spring-based synthetic rock mass models, the intact rock is represented by lattice spring models (LSM) as a random assembly of concentrated point mass particles connected by massless nonlinear springs in three dimensions. Two springs connect the lattice nodes to represent normal and shear contact stiffness. In the LS-SRM method, spherical particles and contacts in PFC are replaced by point masses (nodes) and nonlinear springs, respectively. As in PFC, the movement of lattice nodes is governed by Newton's second law of motion, and the elastic material properties of the model (linear force-displacement relation) determine the stiffness of lattice springs (Cundall and Sainsbury 2011). LS-SRM provides an alternative to BPM and BBM for the simulation of the mechanical behavior of intact rock. The intact rock in a BPM approach is represented as circular/spherical rigid particles bonded together (Potyondy and Cundall 2004). In the BBM approach, the intact rock is simulated as a solid (zero porosity), composed of interlocked irregular polygons to prevent block rotation after contact breakage, as in PFC (Turichshev and Hadjigeorgiou 2017). Both approaches represent pre-existing discontinuities with a discrete fracture network (DFN), and with this approach, the rock mass can be modeled as an anisotropic discontinuum media (Oge 2018).

The LSM code employs an explicit solution scheme, and all nodes in the model are simulated by solving three translations and three rotation equations of motion. More details about the mechanical formulation of the LS-SRM method can be found in the User's Guide and Tutorial

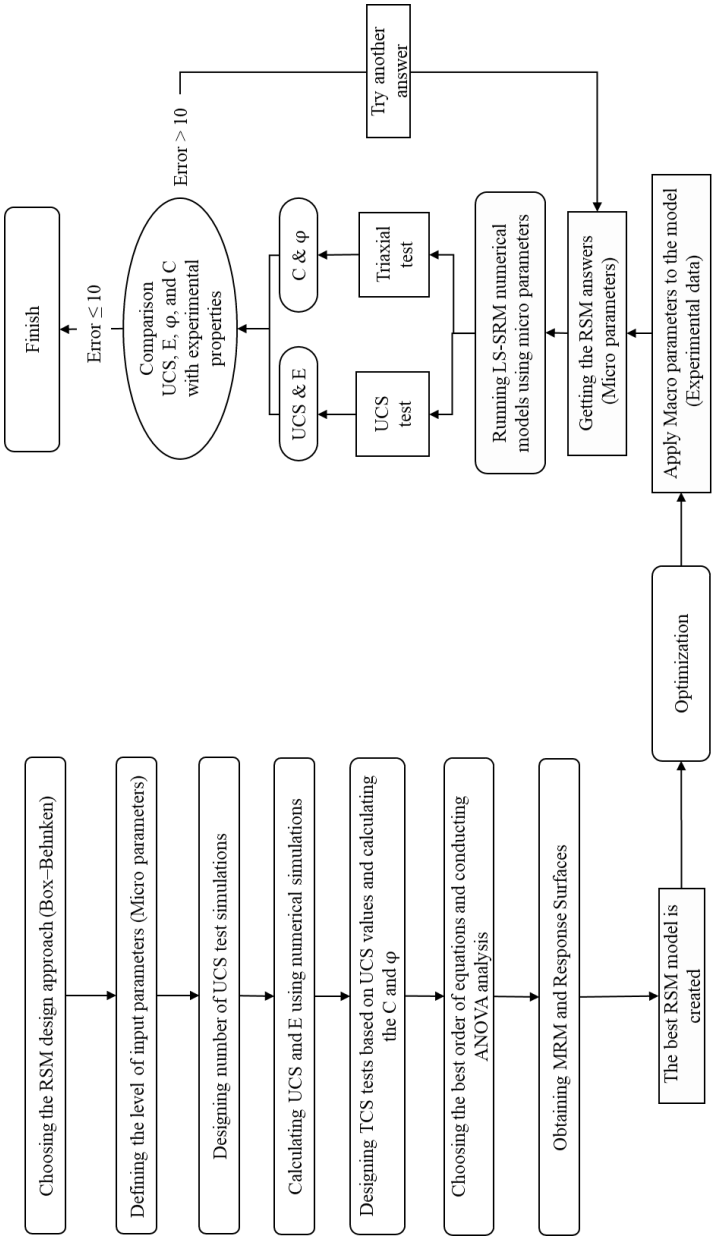

Fig. 1 The framework of the LS-SRM model calibration procedure

(Itasca 2016) and references therein. SRMTools is a recent code developed by Itasca, using the LS-SRM approach like the Slope model (Itasca 2016). In this study, SRMTools is used in the numerical modeling part. Contacts in SRMTools can be simulated either by parallel bonds, which have limitations in simulating rock-like materials (Bastola and Cai 2018b), or flat-joint contacts, representing the contacts between rigid polygonal or polyhedral particles. The flat joint contact prevents nodes from rolling after breaking the main parallel bond. After a flat joint contact is broken, the force-displacement relationships change from a bonded to a fully unbonded and frictional state (Potyondy 2015). Fig. 2 illustrates the parallel spring and sub-springs in SRMTools. It is noted that a minimum of three sub-springs is arranged around the contact disk. The fast-computational time is one of the major advantages of the LSM approach because it is formulated in a small strain that does not require detection and updating of contacts, as in DEM approaches. More details about the mechanical formulation of the LS-SRM method can be found in the Users Guide and Tutorial (Itasca 2016) and references therein.

3. Design of experiments based on response surface methodology (RSM)

The Response Surface Methodology (RSM) was applied to optimize the number of experiments and provide a better understanding of LS-SRM micro parameters affecting the macro properties of the numerical model in an interactive way (Montgomery 2001). RSM adopts a combination of

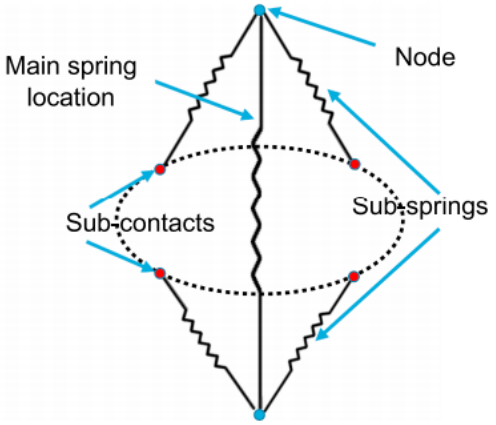

Fig. 2 The flat joint contact in SRMTool (Itasca 2016)

statistical and mathematical approaches to model a process and investigate the interaction of model input parameters that affect the responses. In other words, RSM is a multivariate statistical approach that can evaluate the impacts of model input parameters on the model output parameters and design enough tests. The Box–Behnken Design was utilized in this study to model RSM (Heidarzadeh *et al*. 2017). This method can model the relationship between the range of model input and model output parameters. In this study, the model input parameters are lattice parameters; UCS_m, E_m, T_m, and φ_m. Macro parameters of a rock sample, such as UCS, E, cohesion, and φ, are the model output parameters. The mathematical relationship of the response on these parameters can be approximated by the quadratic (second degree) polynomial equation as follows (Asadizadeh *et al.* 2018, Babanouri *et al.* 2020, Li *et al.* 2020)

$$y = \beta_0 + \sum_{i=1}^{3} \beta_i X_i + \sum_{i=1}^{3} \beta_{ii} X_i^2 + \sum_{i=1}^{3} \sum_{j=i+1}^{3} \beta_{ij} X_i X_j \quad (1)$$

where y is a response or a model output variable (UCS, E, cohesion, and φ), β_{ii}, β_{ij}, β_i, and β_0 are the regression coefficients, and X_i and X_j are the values of model input parameters (UCS_m, E_m, T_m, and φ_m) coded according to

$$X_i = \frac{x_i - x_0}{\Delta x} \quad (2)$$

where x_0 is the value of x_i at the center point, and Δx is the variation interval. According to Box- Behnken design, the codes, and the levels of model input parameters in this study are selected by considering the extreme parameters. Table 1 presents these model input variables and their corresponding levels. Four model input parameters and three levels were defined to focus response surface methodology on the range of -1 to 1. Preliminary numerical simulations defined the levels of each model input parameter. It should be noted that, in calibration studies, the micro-scale or lattice parameters are frequently higher than the values in the macro-scale. Therefore, the upper boundaries of the Box–Behnken parameters (250 MPa UCS, 200 GPa E_m, 25 MPa T_m, and 65° φ_m) should not be compared with actual macro-scale rock parameters.

Table 1 Coded model input variables and their corresponding levels obtained from Box–Behnken design

Variable/Parameter/Factor	Code	Level		
		-1	0	1
Lattice uniaxial compressive strength (MPa)	UCS_m	20	135	250
Lattice elastic modulus (GPa)	E_m	4	102	200
Lattice tensile strength (MPa)	T_m	2	13.5	25
Flat joint friction angle (degree)	φ_m	10	37.5	65

3.1 Test simulations

The SRMTool was employed to generate and execute the models to evaluate the relationship between LS-SRM micro and macro properties. In total, 29 uniaxial and 58 triaxial test simulations were carried out in the scope of this study.

Rectangular prism specimens of 54 mm ×54 mm ×120 mm were generated with three axial and six lateral force and displacement monitoring points. The lattice resolution, the ratio of the shortest dimension of the specimen to the size of the lattice (with the same unit), has a significant impact on model behavior. Itasca recommended that the minimum lattice resolution of 20 is suitable for SRMTool models. Therefore, the lattice size of 2.0 mm was assigned to obtain a lattice resolution of 27 in models of this study. Voronoi lattice and spherical lattice models are two available lattice models in the SRMTool model. It has been reported that the triaxial test simulations performed with Voronoi lattice models give unrealistic stress-strain curves above 10 MPa confinement levels (Bastola and Cai 2018b). In addition, the computational time is longer for the Voronoi lattice model; therefore, the spherical lattice model is preferred in this study.

It is shown by Bastola and Cai (2018b) that the parallel bond model has limitations in simulating rock-like materials. Therefore, in this study, the flat joint model was applied for realistic simulations of uniaxial compressive strength (σ_c) and σ_c/σ_t ratios of intact rock. The radius multiplier is flat joint contact diameter ration to the particle diameter. This multiplier should be less than 1.0 for the triaxial simulation (Itasca 2016). As the value of the radius multiplier decreases, the computation time increases exponentially; a disk radius multiplier of 0.9 with three contact points is used in this study. According to Bastola and Cai (2019), the loading rate does not significantly affect the macro-mechanical properties of the model. In order to maintain the quasi-static equilibrium, the tests are conducted by applying a constant vertical displacement rate (velocity) of 0.01 m/s at the top of the specimen. The density and the porosity are input lattice parameters used to calibrate the model. The studied rock densities range from 2500 to 2800 kg/m^3 and have around 0.3% porosity. Our simulations found that ±150 kg/m3 variation in rock density has almost zero impact on estimated macro-scale model parameters. Therefore, for simplicity, we consider a constant rock density of 2650 kg/m3 and 0.3% porosity in this study.

Generated specimen geometry with lattice spring

Table 2 LS-SRM model inputs and obtained UCS simulation results

Model No.	Micro Parameters (Lattice Parameters)				Macro Parameters (UCS model results)	
	UCS_m (MPa)	E_m (GPa)	T_m (MPa)	φ_m (°)	UCS (MPa)	E (GPa)
1	135	102	2	65	514	74
2	135	102	25	65	354	75
3	250	102	25	37.5	355	75
4	135	200	13.5	65	432	147
5	135	200	25	37.5	158	147
6	250	4	13.5	37.5	367	3
7	20	102	25	37.5	84	75
8	135	4	25	37.5	157	3
9	250	102	13.5	65	875	75
10	135	4	13.5	65	433	3
11	135	102	25	10	102	75
12	20	102	2	37.5	28	75
13	135	4	2	37.5	217	3
14	135	102	13.5	37.5	191	75
15	20	200	13.5	37.5	46	147
16	135	102	13.5	37.5	191	75
17	135	102	13.5	37.5	190	75
18	20	102	13.5	65	100	75
19	135	4	13.5	10	120	3
20	20	4	13.5	37.5	45	3
21	250	102	13.5	10	238	75
22	20	102	13.5	10	30	75
23	135	102	13.5	37.5	192	75
24	135	102	2	10	137	75
25	135	102	13.5	37.5	188	75
26	135	200	13.5	10	123	147
27	135	200	2	37.5	215	146
28	250	200	13.5	37.5	380	147
29	250	102	2	37.5	394	75

connections and force-displacement monitoring points are presented in Fig. 3. For stress and strain calculations, the average values of the relevant monitoring points are considered.

3.1.1 UCS test simulations

The optimum number of UCS experiments to be simulated was decided by the Box-Behnken design method as described in section 3. By optimizing the lattice scale micro-parameter levels used in models, 29 experimental UCS simulations were determined to be required for this study. At the end of these simulations, UCS and Young's modulus values were calculated for each model by plotting stress vs. axial strain curves (see Fig. 4) using the data collected from the monitoring points. Model input parameters (lattice parameters) and UCS simulation results are presented in Table 2. After ensuring that the data obtained from UCS simulations are sufficient to be used in Analysis of Variance (ANOVA) and Multiple Regression Modelling (MRM) analyses, triaxial compressive strength (TCS) test simulations were started.

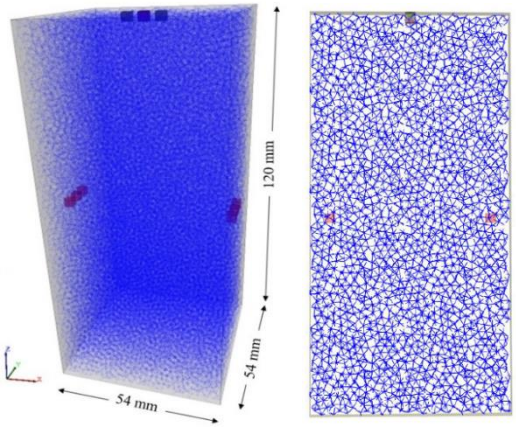

Fig. 3 Generated LS-SRM model with axial-lateral monitoring points and lattice spring connections

3.1.2 TCS test simulations

TCS simulations were carried out in two different confinement levels for each model. The same model geometry and monitoring points as in the UCS part are used

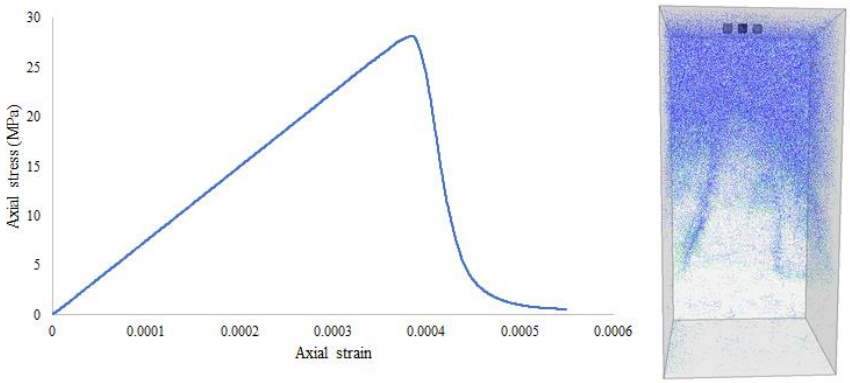

Fig. 4 Axial stress–axial strain curve of the model with UCSm of 20 MPa, E_m of 102 GPa, φ_m of 37.5, and T_m of 2 MPa under UCS test

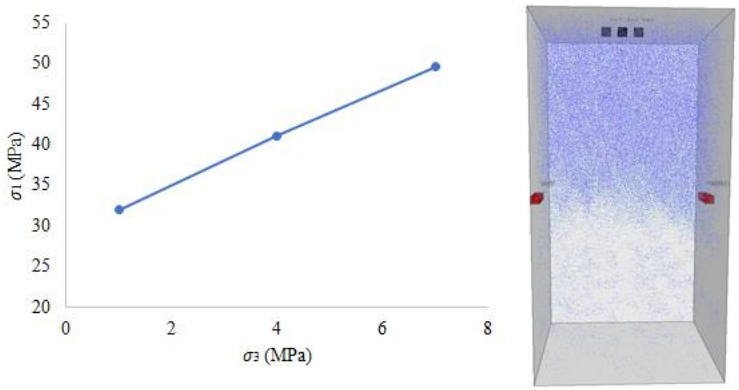

Fig. 5 Mohr-Coulomb strength envelope for the model with UCS_m of 20 MPa, E_m of 102 GPa, φ_m of 37.5, and T_m of 2 MPa under TCS test

Table 3 TCS model results

Model No.	Cohesion (MPa)	Friction angle (°)	Model No.	Cohesion (MPa)	Friction angle (°)	Model No.	Cohesion (MPa)	Friction angle (°)
1	121.5	62.1	**11**	45.3	7.4	**21**	119.3	0.00
2	28.5	70.2	**12**	8.6	29.4	**22**	14.3	3.3
3	114.1	26.8	**13**	91.7	15.1	**23**	55.5	30.4
4	34.8	70.2	**14**	56.7	29.8	**24**	64.1	7.4
5	46.2	29.9	**15**	13.7	28.6	**25**	56.7	29.8
6	127.7	21.4	**16**	55.5	30.4	**26**	44.1	16.6
7	25.2	28.7	**17**	57.9	29.6	**27**	64.0	30.8
8	69.8	10.9	**18**	7.5	70.5	**28**	105.7	32.6
9	86.1	68.4	**19**	56.5	2.4	**29**	112.4	33.1
10	66.3	49.8	**20**	13.6	28.6			

in these simulations. Parameters such as the radius multiplier, lattice size, and displacement rate are also kept constant. At the end of the simulations, Mohr-coulomb strength envelopes were plotted as shown in Fig. 5 (three data used for each model), and the cohesion and friction angle values were obtained. TCS simulation results are presented in Table 3.

3.2 Analysis of variance (ANOVA)

To evaluate the effect of each variable and their mutual contribution to the response, the analysis of variance (ANOVA) approach was employed (Montgomery 2001). The statistical properties of the proposed models are shown in Table 4.

The actual and predicted values of all four models that indicate a linear regression relationship are shown in Fig. 6.

During the process of responses using ANOVA if the error (residuals) is a function of the response, transformation of response is necessary (Montgomery, 2001). The normal residual plot controls the normality, meaning that response transformation is necessary if there is a pattern in the chart of residuals versus predicted response values. Unless the maximum response to the minimum

Table 4 Statistical properties of the RSM models

Description / Model	UCS	E	Cohesion	Friction angle	Statistical parameter
Model is significant	170.20	380666.02	3.62	151.92	F-value
	< 0.0001	< 0.0001	< 0.0001	< 0.0001	P-Value
Model is applicable for the design space	51.313	1757.209	18.4817	39.9854	Adequate precision
A high correlation between the input and output values	0.9789	1.000	08796	0.9620	R^2
In good agreement with their R^2 coefficient	0.9732	1.000	0.8535	0.9557	Adjusted-R^2

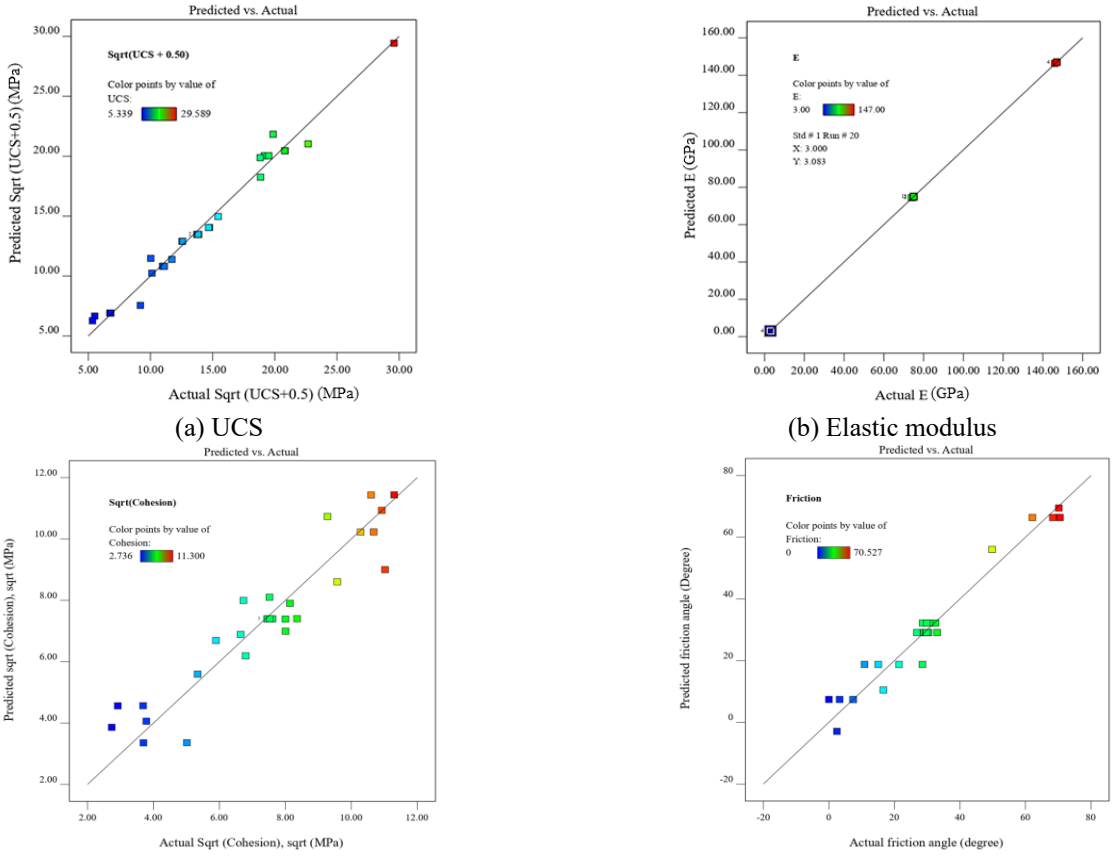

(a) UCS (b) Elastic modulus

(c) Cohesion (d) Friction angle

Fig. 6 The actual and predicted values of (a) UCS, (b) Elastic Modulus, (c) Cohesion and (d) Friction angle models

response ratio is large, transforming the response will not make a significant difference (Miller 1984). The normal percentage probability versus the studentized residual of the model was plotted for all four parameters, as shown in Fig. 7. It is observed that the data transformation for UCS and cohesion is necessary.

The Box-Cox plot is another method to check the necessity of response transformation, and this method can also provide a guideline for selecting the most suitable transformation (Montgomery 2001). A transformation is recommended based on the best lambda value, which is found at the curve's minimum point generated by the natural log of the sum of squares of the residuals. If the 95% confidence interval around this lambda includes 1, this method does not recommend a specific transformation. The Box-Cox plot (See Fig. 8) provides a recommended transformation from the root square family for UCS, and cohesion as follows

$$UCS_{Transformed} = \sqrt{UCS_{Untransformed+k}}, k = 0.5 \quad (3)$$

$$Cohesion_{Transformed} = \sqrt{Cohesion_{Untransformed}} \quad (4)$$

3.3 Multiple Regression Modeling (MRM)

Various multiple regression modeling equations were analyzed using Analysis of Variance (ANOVA) techniques for all four models, see Table 5. The ANOVA calculations for multiple regression are very similar to the calculations

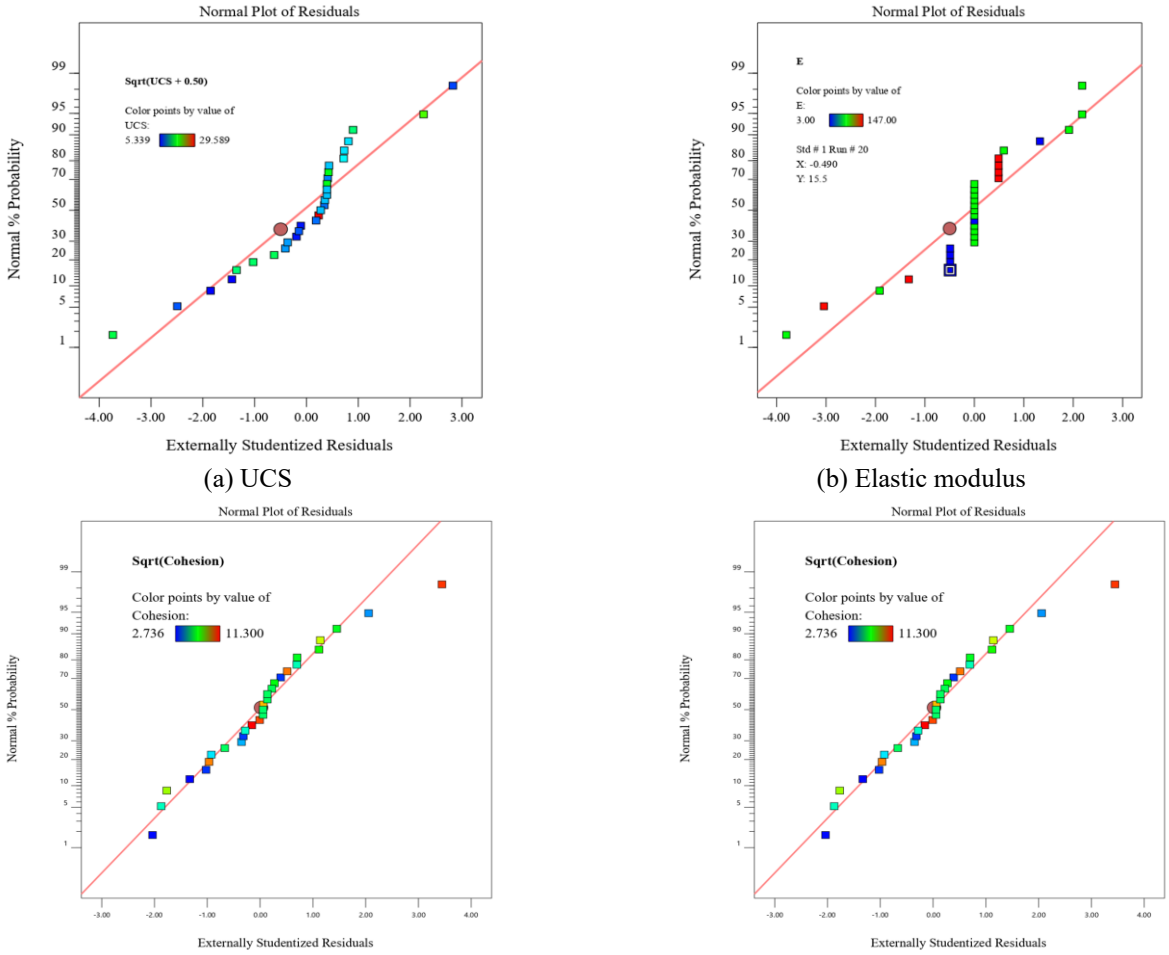

Fig. 7 Normal probability plot for (a) UCS, (b) Elastic modulus, (c) Cohesion, and (d) Friction angle models

for simple linear regression, but the degrees of freedom are adjusted to reflect the number of explanatory variables included in the model.

The nonlinear models for the model output parameters (UCS, E, cohesion, φ) were estimated as the functions of the model input parameters (UCS_m, E_m, T_m, φ_m,) using presented simulation results from Table 1 and 2 through the best fits to Equation 1. The final mathematical model is presented in terms of actual factors for all models as follows

$$Sqrt\,(UCS + 0.5) = 6{,}07273 + 0.040908 \times UCS_m + 0.074071 \times T_m - 0.141730 \times \varphi_m - 0.000919 \times UCS_m \times T_m + 0.000762 \times UCS_m \times \varphi_m - 0.002854 \times \varphi_m^2 \quad (5)$$

$$E = 0.028085 + 0.730849 \times E_m + 0.026897 \times T_m + 0.000222 \times E_m \times T_m - 0.000027 \times T_m \times \varphi_m - 0.001260 \times T_m^2 \quad (6)$$

$$Sqrt(Cohesion) = 3.06895 + 0.029873 \times UCS_m - 0.006174 \times E_m + 0.078503 \times T_m + 0.043456 \times \varphi_m - 0.003486 \times \varphi_m \times T_m \quad (7)$$

$$\varphi = -7.52140 + 0.14569 \times E_m + 0.298716 \times \varphi_m - 0.000387 \times E_m^2 + 0.010317 \times \varphi_m^2 \quad (8)$$

The proposed equations can offer guidance for the numerical studies that may be conducted in the future. Predictions about the output for each level of factors can be made by utilizing the equation in terms of actual factors.

4. Analysis of response surface models

4.1 Effects of model input parameters on UCS

In order to examine the effect of each variable on the response, the studied model parameter (UCS) was varied while all other parameters were kept at their middle values. The impact of UCS_m, E_m, T_m, and φ_m on macro-scale uniaxial compressive strength (UCS), is presented in Fig. 9(a). An increase in UCS_m within the range of 20 MPa to 250 MPa, leads to a more than 700% nonlinear increase in UCS. This considerable increase shows that UCS_m is a heavily impacting parameter on the UCS. Similarly, with increasing the φ_m from 10° to 65°, UCS also increases non-linearly by 252%. The increase of T_m from 2 MPa to 25

Table 5 ANOVA for the models of macro parameters based on RSM

	Parameters	Sum of Squares	Degree of freedom	Mean Square	F-Value	P-value	Significance
UCS	Model	861.87	6	143.64	170.20	< 0.0001	Significant
	UCS_m	517.23	1	517.23	612.85	< 0.0001	
	T_m	3.97	1	3.97	4.70	0.0413	
	φ_m	278.74	1	278.74	330.28	< 0.0001	
	$UCS_m \times T_m$	5.91	1	5.91	7.00	0.0148	
	$UCS_m \times \varphi_m$	23.25	1	23.25	27.55	< 0.0001	
	φ_m ^2	32.78	1	32.78	38.84	< 0.0001	
	Residual	18.57	22	0.8440			
	Cor Total	880.43	28				
E	Model	62065.11	5	12413.02	3.807E+05	< 0.0001	Significant
	E_m	62064.08	1	62064.08	1.903E+06	< 0.0001	
	T_m	0.3333	1	0.3333	10.22	0.0040	
	$E_m \times T_m$	0.2500	1	0.2500	7.67	0.0109	
	$T_m \times \varphi_m$	0.2500	1	0.2500	7.67	0.0109	
	T_m ^2	0.1954	1	0.1954	5.99	0.0224	
	Residual	0.7500	23	0.0326			
	Cor Total	62065.86	28				
Cohesion	Model	155.33	5	31.07	33.62	< 0.0001	Significant
	UCS_m	141.63	1	141.63	153.27	< 0.0001	
	E_m	4.39	1	4.39	4.75	0.0397	
	T_m	4.33	1	4.33	4.69	0.0410	
	φ_m	0.1182	1	0.1182	0.1279	0.7239	
	$T_m \times \varphi_m$	4.86	1	4.86	5.26	0.0313	
	Residual	21.25	23	0.9240			
	Cor Total	176.58	28				
friction angle	Model	11554.24	4	2888.56	151.92	11554.24	Significant
	E_m	539.35	1	539.35	28.37	539.35	
	φ_m	10438.93	1	10438.93	549.02	10438.93	
	E_m ^2	91.19	1	91.19	4.80	91.19	
	φ_m ^2	420.18	1	420.18	22.10	420.18	
	Residual	456.33	24	19.01			
	Cor Total	12010.57	28				

MPa leads to a reduction of UCS by 15%. Moreover, E_m has no apparent effect on UCS.

Fig. 9(b) presents the changes in UCS due to the variation of T_m and UCS_m simultaneously when φ_m and E_m were kept constant. As is shown, with the increase of UCS (20 MPa to 250 MPa) and T_m (2 MPa to 25 MPa), UCS increased by 712%. Furthermore, at higher UCS_m levels, when T_m increased from 2 MPa to 25 MPa, UCS was reduced by 30%. At lower UCS_m levels, UCS increased around 50%. When T_m was kept constant (2 MPa), an increase in UCS_m from 20 MPa to 250 MPa led to an increase in UCS by ten times its original value. At T_m=25 MPa, this increase was around 470%.

Fig. 9(c) shows the mutual effect of φ_m and UCS_m on UCS. In each plot, two parameters are varied while the others are held constant at their middle levels. According to Fig. 9(b), when E_m and T_m were kept constant (102 GPa and 13.5 MPa), as φ_m and UCS_m increased, UCS increased by 1802 % (from 46 MPa to 875 MPa). This implies that both φ_m and UCS_m had a positive and significant impact on UCS. Furthermore, at higher levels of UCS_m, an increase of φ_m from 10° to 60° leads to an increase on UCS by 287%, while UCS increased by 197% at lower levels. Also, when φ_m was kept constant at 10°, UCS_m increased from 20 to 250 MPa.

4.2 Effects of model input parameters on the elastic modulus

The effect of UCS_m, E_m, T_m and φ_m on macro-scale elastic modulus (E) is presented in Fig. 10(a). It can be seen that UCS_m, T_m, and φ_m have no effect on E. E_m strongly affected E in which an increase in E_m from 4 GPa to 200 GPa increased E around the same order of magnitude. Fig. 10(b) shows the variation of E due to the effect of E_m and UCS_m while two other parameters (φ_m and T_m) were kept constant. As shown, the variation of UCS_m did not affect E, while it was highly affected by E_m.

4.3 Effects of model input parameters on cohesion

The effect of four variables on cohesion is presented in this part by keeping other variables constant at their middle levels. The effect of UCS_m, E_m, T_m and φ_m on cohesion is

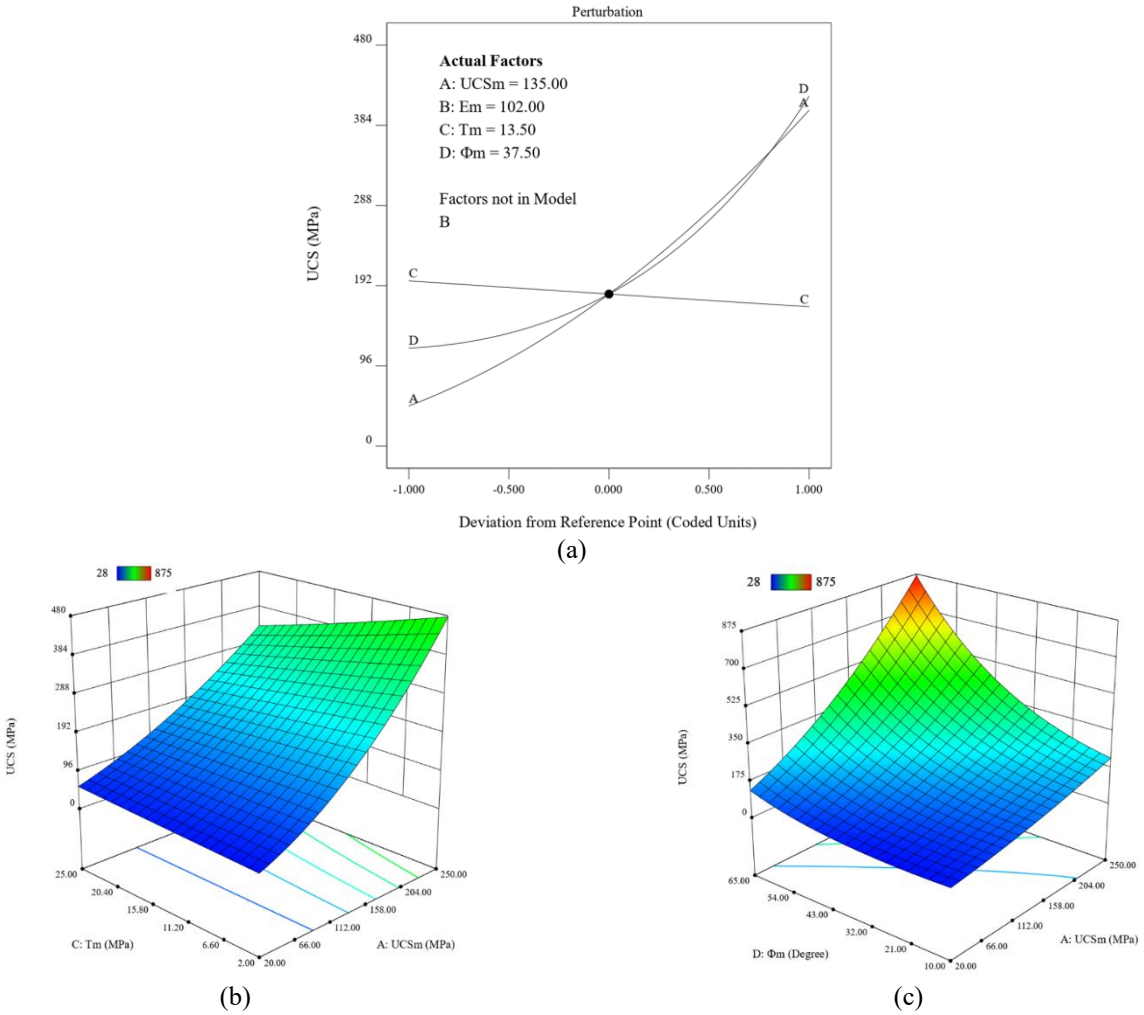

(a) (b) (c)

Fig. 9 (a) The effect of UCS_m, E_m, T_m and φ_m on UCS in terms of coded value, (b) response surface and contour plot of the mutual effect of T_m and UCS_m on UCS and (c) Response surface and contour plot of the mutual effect of φ_m and UCS_m on UCS

I

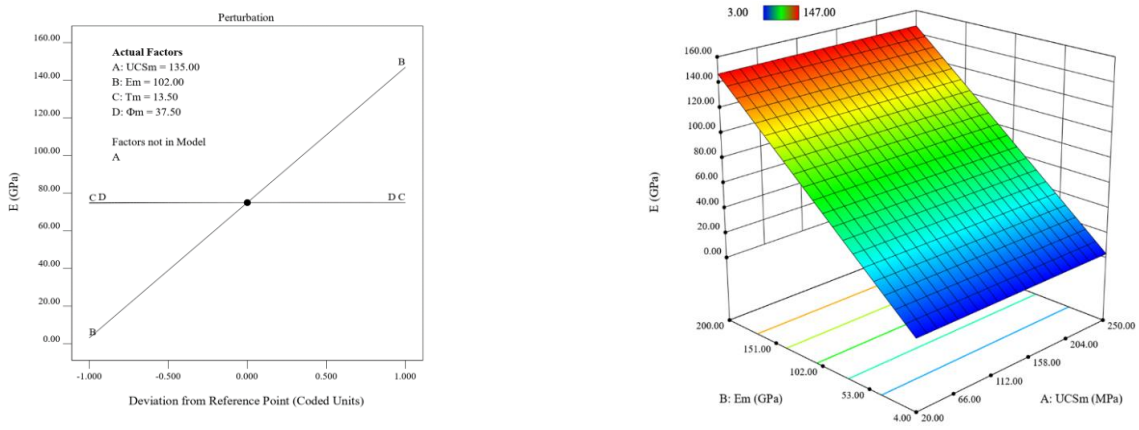

(a) (b)

Fig. 10 (a) The effect of UCS_m, E_m, T_m and φ_m on E in terms of coded value and (b) response surface and contour plot the mutual effect of T_m and E_m on E

presented in Fig. 11(a). As UCS_m increased from 20 MPa to 250 MPa, cohesion also increases non-linearly around six times, which shows UCS_m has a crucial effect on cohesion. In contrast, when E_m and T_m increased from minimum to maximum, the cohesion was reduced by 27%. Also, changes in φ_m did not significantly affect cohesion.

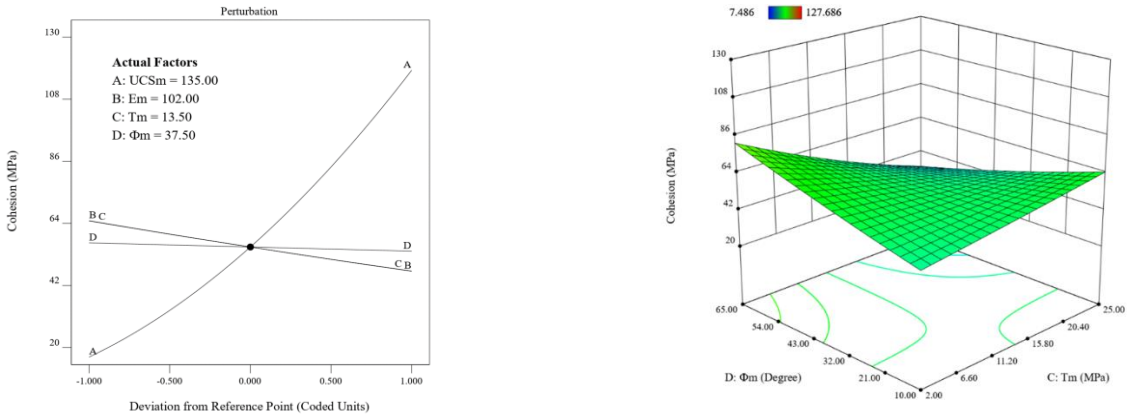

(a) (b)

Fig. 11 (a) the effect of UCS_m, E_m, T_m and φ_m on cohesion in terms of coded value and (b) response surface and contour plot, the mutual effect of T_m and φ_m on cohesion

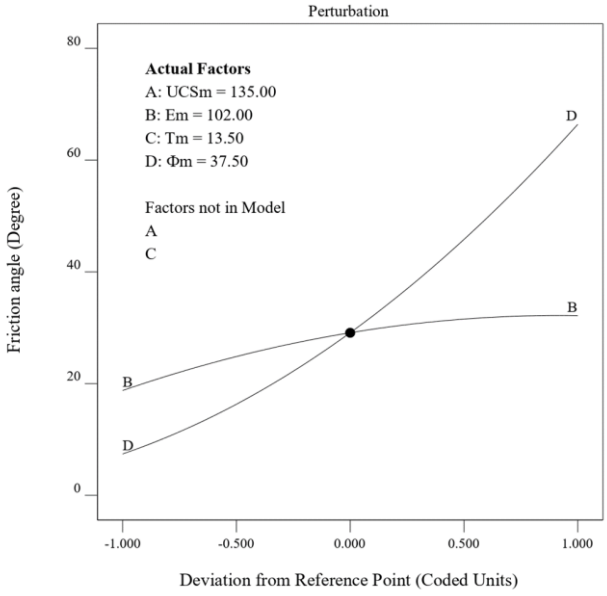

Fig. 12 The effect of UCS_m, E_m, T_m and φ_m on the φ in terms of coded value

Fig. 11(b) shows the variation of cohesion due to the changes in T_m and φ_m, when UCS_m and E_m were kept constant. As shown, when φ_m was kept at 10°, with the increase of T_m from 2 MPa to 25 MPa, cohesion increased from 45 MPa to 65 MPa (30%). When φ_m was 65°, this amount decreased by 61%. Furthermore, at high levels of T_m, by increasing φ_m from 10° to 65°, cohesion reduced by 51%, and at minimum levels of T_m, cohesion increased by 64%. In other words, the considerable variation in T_m and φ_m, causes slight changes in cohesion.

4.4 Effects of model input parameters on friction angle

The impact of UCS_m, Em, T_m and φ_m on macro-scale flat joint friction angle (j) is presented in Fig. 12. It was found that UCS_m and T_m have no apparent effect on j. However, as E_m and φ_m increase, j increased by 71% and 797%, respectively. It should be noted that the input parameters did not have a mutual effect on each other for this case. It was concluded that φ_m governs the φ.

5. Optimization and validation

Response surface methodology (RSM) was adopted as an optimization method to search for a combination of factor levels that simultaneously satisfies the criteria placed on each response and factor. Equations 5 to 8 were employed to include the responses in the optimization criteria. In other words, numerical optimization uses the models to search the factor space for the best trade-offs to achieve multiple goals. In this part, five different rock properties ranging from weak to strong were used as targets to optimize the best lattice properties, which were used as input parameters for numerical models (see Table 6). As a result of numerical models and validation of the RSM models, numerical model outputs were compared with

Table 6 RSM model validation

Rock type	Lattice parameters (Micro parameters)				Macro parameters				Models and errors
	UCS_m (MPa)	Young's modulus (GPa)	Tensile strength (MPa)	Friction angle (°)	UCS (MPa)	Young's modulus (GPa)	Cohesion (MPa)	Friction angle (°)	
Limestone	36.24	48.71	2.05	45.80	70.00	35.60	19.77	34.00	RSM
					70.00	35.60	20.50	34.00	Experimental (Karanam *et al.* 2009)
					64.70	36.00	17.00	36.00	Numerical
					8.19	**1.12**	**16.29**	**5.56**	Error%
Limestone	56.00	64.89	2.45	49.54	110.00	47.40	25.37	40.45	RSM
					110.00	47.40	26.67	45.00	Experimental (Karanam *et al*. 2009)
					111.61	47.10	25.32	41.97	Numerical
					1.44	**0.64**	**0.20**	**3.62**	Error%
Limestone	80.57	71.45	2.34	49.34	152.00	52.20	33.30	40.81	RSM
					152.00	52.20	33.30	46.00	Experimental (Karanam *et al*. 2009)
					161.68	52.03	35.23	43.34	Numerical
					5.99	**0.33**	**5.48**	**5.84**	Error%
Granite	94.57	92.89	11.29	54.10	206.23	68.20	38.24	48.40	RSM
					205.70	68.20	38.30	49.10	Experimental (Hu *et al*. 2020)
					186.40	68.10	36.84	46.81	Numerical
					10.64	**0.15**	**3.80**	**3.40**	Error%
Gabbro	147.98	152.10	11.73	51.04	300.90	111.70	57.80	48.00	RSM
					300.90	111.70	57.80	48.00	Experimental (Hu *et al.* 2020)
					288.90	111.70	61.43	45.14	Numerical
					4.15	**0.00**	**5.91**	**6.34**	Error%

experimental data, and the percentage errors of models for each parameter were presented. According to Table 6, relatively small percent errors (less than 11%) were obtained. It was concluded that the presented RSM model (Eqs. (5)-(8)) could be used to calibrate rock samples on the lab scale.

6. Conclusions

This paper proposed a robust approach for LS-SRM model calibration using RSM. The experiments were designed using the Box–Behnken Design method and 29 UCS and 58 TCS test simulations were performed. For this purpose, a wide range of micro-mechanical lattice parameters (UCS_m, E_m, T_m, and φ_m) were selected, and models were simulated using SRMTools software. Four model outputs, mainly UCS, E, cohesion, and φ were calculated using stress-strain curves and mohr-coulomb strength envelopes. The results revealed that UCS_m and φ_m are the most effective parameters on the macro-scale UCS. Whereas T_m has a slight effect and E_m has no apparent effect on macro-scale UCS. Additionally, T_m, UCS_m, φ_m have a mutually significant impact on UCS. E_m strongly affected elastic modulus, while other parameters have very slight or no effects on E. UCS_m, and E_m are found as the most significant parameters for macro-scale cohesion. However, φ_m does not have a significant effect on cohesion. In this regard, T_m and φ_m mutually affect the cohesion parameter. For φ, φ_m mainly controls this parameter, and E_m is found to have a secondary effect on φ. T_m and UCS_m were found to have no apparent effect on φ. The calculated models were used to optimize the best input array for numerical models so that their outputs approximate lab tests. Finally, the proposed RSM models were evaluated using various rock types ranging from weak to strong. The validation study results showed that this model could be used to calibrate LS-SRM models on the lab scale.

Declaration of competing interest

The authors wish to confirm that there are no known conflicts of interest associated with this publication, and there has been no significant financial support for this work that could have influenced its outcome.

References

Asadizadeh, M., Moosavi, M. and Hossaini, M.F. (2018), "Investigation of mechanical behaviour of non-persistent jointed blocks under uniaxial compression", *Geomech. Eng.*, **14**(1), 29-42**.** https://doi.org/10.12989/gae.2018.14.1.029.

Babanouri, N., Asadizadeh, M. and Hasan-Alizade, Z. (2020),

"Modeling shear behavior of rock joints: A focus on interaction of influencing parameters", *Int. J. Rock Mech. Min. Sci.*, **134**. https://doi.org/10.1016/j.ijrmms.2020.104449.

Barla, M., Piovano, G. and Grasselli, G. (2012), "Rock slide simulation with the combined finite-discrete element method", *Int. J. Geomech.*, **12**(6), 711-721. https://doi.org/10.1061/(asce)gm.1943-5622.0000204.

Bastola, S. and Cai, M. (2018a), "Investigation of strength and deformation behaviors of intact and jointed granite using lattice-spring-based synthetic rock mass models", *Proceedings of the 2nd International Discrete Fracture Network Engineering Conference*, DFNE 2018.

Bastola, S. and Cai, M. (2018b), "Simulation of stress–strain relations of Zhenping marble using lattice-spring-based synthetic rock mass models", *Proceedings of the 52nd U.S. Rock Mechanics/Geomechanics Symposium*.

Bastola, S. and Cai, M. (2019), "Investigation of mechanical properties and crack propagation in pre-cracked marbles using lattice-spring-based synthetic rock mass (LS-SRM) modeling approach", *Comput. Geotech.*, **110**, 28-43. https://doi.org/10.1016/j.compgeo.2019.02.009.

Brideau, M.A., Pedrazzini, A., Stead, D., Corey, I., Jaboyedoff, M. and Van Zeyl, D. (2011), "Three-dimensional slope stability analysis of South Peak, Crowsnest Pass, Alberta, Canada", *Springer*, **8**, 139-158. https://doi.org/10.1007/s10346-010-0242-8.

Camones, L.A.M., Vargas, E. do A., de Figueiredo, R.P. and Velloso, R.Q. (2013), "Application of the discrete element method for modeling of rock crack propagation and coalescence in the step-path failure mechanism", *Eng. Geol.*, **153**, 80-94. https://doi.org/10.1016/j.enggeo.2012.11.013.

Chehreghani, S., Noaparast, M., Rezai, B. and Shafaei, S.Z. (2017), "Bonded-particle model calibration using response surface methodology", *Particuology*, **32**, 141-152. https://doi.org/10.1016/j.partic.2016.07.012.

Cundall, A.P. (1971), "A computer model for simulating progressive, large-scale movement in blocky rock system", *Proceedings of the International Symposium on Rock Mechanics.*

Cundall, A.P., and Sainsbury, D. (2011), "Lattice method for modeling brittle, jointed rock, in continuum and distinct element modeling in geomechanics", 12-01, 649-660.

Cundall, A.P., Damjanac, B. and Varun, V. (2016), "Considerations on slope stability in a jointed rock mass", *Proceedings of the 50th US Rock Mechanics / Geomechanics Symposium.*

Dadashzadeh, N., Duzgun, H.S.B. and Yesiloglu-Gultekin, N. (2017), "Reliability-based stability analysis of rock slopes using numerical analysis and response surface method", *Rock Mech. Rock Eng.*, **50**(8), 2119-2133. https://doi.org/10.1007/s00603-017-1206-2.

Di, S.J., Xu, W.Y., Ning, Y., Wang, W. and Wu, G.Y. (2011), "Macro-mechanical properties of columnar jointed basaltic rock masses", *J. Central South University of Technology (English Edition)*, **18**(6), 2143-2149. https://doi.org/10.1007/s11771-011-0955-4.

Eberhardt, E., Stead, D., Coggan, J.S. and Willenberg, H. (2003), "Hybrid finite-/discrete-element modelling of progressive failure in massive rock slopes", *Proceedings of the 10th ISRM Congress*.

Elmo, D. and Stead, D. (2010), "An integrated numerical modelling-discrete fracture network approach applied to the characterisation of rock mass strength of naturally fractured pillars", *Rock Mech. Rock Eng.*, **43**(1), 3-19. https://doi.org/10.1007/s00603-009-0027-3.

Farahmand, K., Vazaios, I., Diederichs, M.S. and Vlachopoulos, N. (2018), "Investigating the scale-dependency of the geometrical and mechanical properties of a moderately jointed rock using a synthetic rock mass (SRM) approach", *Comput. Geotech.*, **95**, 162-179. https://doi.org/10.1016/j.compgeo.2017.10.002.

Gen-Hua, S. (1989), "Discontinuous deformation analysis a new numerical model for the static and dynamics of block systems", *PhD Dissertation, Dept. of Civil Engineering*.

Griffiths, D.V. and Fenton, G.A. (2004), "Probabilistic slope stability analysis by finite elements", *J. Geotech. Geoenviron. Eng.*, **130**(5), 507-518. https://doi.org/10.1061/(asce)1090-0241(2004)130:5(507).

Havaej, M. and Stead, D. (2016), "Investigating the role of kinematics and damage in the failure of rock slopes", *Comput. Geotech.*, ***78***, 181-193. https://doi.org/10.1016/j.compgeo.2016.05.014.

Heidarzadeh, S, Saeidi, A. and Rouleau, A. (2017), "Assessing the effect of open stope geometry on rock mass brittle damage using a response surface methodology", *Int. J. Rock Mech. Min. Sci.*, **106**, 60-73. https://doi.org/10.1016/j.ijrmms.2018.03.015.

Herrero, C. (2015), "Quantifying the effect of in-situ stresses and pit depth on slope stability by incorporating brittle fracturing in numerical model analyses", *PhD thesis, Colorado School of Mines.*, 194p.

Hu, L., Ghassemi, A., Pritchett, J., Garg, S. and Ishido, T. (2020), "Self-potential response in laboratory scale EGS stimulation", *Rock Mech. Rock Eng.*, **53**(2), 691-703. https://doi.org/10.1007/s00603-019-01937-y.

Huang, D., Cen, D., Ma, G. and Huang, R. (2015), "Step-path failure of rock slopes with intermittent joints", *Landslides*, **12**(5), 911-926. https://doi.org/10.1007/s10346-014-0517-6.

Huang, J., Griffiths, D.V. and Fenton, G.A. (2010), "System reliability of slopes by RFEM", *Soils Found.*, **50**(3), 343-353. https://doi.org/10.3208/sandf.50.343.

Itasca Consulting Group (2016), SRMTools - User's Guide and Tutorial. SRMTools - Minneapolis, MN, US.

Itasca Consulting Group. (2019), UDEC, User's Manual Version 5.0. Inc., Minneapolis, MN, US.

Jiang, S.H., Li, D.Q., Zhou, C.B. and Zhang, L.M. (2014), "Capabilities of stochastic response surface method and response surface method in reliability analysis", *Struct. Eng. Mech.*, **49**(1), 111-128. https://doi.org/10.12989/sem.2014.49.1.111.

Jing, L. (2003), "A review of techniques, advances and outstanding issues in numerical modelling for rock mechanics and rock engineering", *Int. J. Rock Mech. Min. Sci*., **40**(3), 283-353. https://doi.org/10.1016/S1365-1609(03)00013-3.

Johnstone, M.W. and Ooi, J.Y. (2010), "Calibration of DEM models using rotating drum and confined compression measurements", *Proceedings of the 6th World Congress on Particle Technology*, Nuremberg, Germany.

Karanam, U., Sunwoo, C., Ochoi, S., Chung, S.K. and Reddy, D.V. (2009), "Empirical approaches for designing wide underground openings–A case study", *Indexed in Chemical Abstracts–CAS Ref. No.: 172238*, 467.

Li, D, Chen, Y., Lu, W. and Zhou, C. (2011), "Stochastic response surface method for reliability analysis of rock slopes involving correlated non-normal variables", *Comput. Geotech.*, **38**(1), 58-68. https://doi.org/10.1016/j.compgeo.2010.10.006.

Li, D, Li, Y., Asadizadeh, M., Masoumi, H. and Hagan, P.C. (2020), "Assessing the mechanical performance of different cable bolts based on design of experiments techniques and analysis of variance", *Int. J. Rock Mech. Min. Sci.*, **130**, 104307. https://doi.org/10.1016/j.ijrmms.2020.104307.

Li, D.Q., Jiang, S.H., Cheng, Y.G. and Zhou, C.B. (2013), "A comparative study of three collocation point methods for odd order stochastic response surface method", *Struct. Eng. Mech.*, **45**(5), 595-611. https://doi.org/10.12989/sem.2013.45.5.595.

Li, D.Q., Qi, X.H., Phoon, K.K., Zhang, L.M. and Zhou, C.B.

(2014), "Effect of spatially variable shear strength parameters with linearly increasing mean trend on reliability of infinite slopes", *Struct. Saf.*, **49**, 45-55. https://doi.org/10.1016/j.strusafe.2013.08.005.

Li, X., Huai, Z., Konietzky, H., Li, X. and Wang, Y. (2018), "A numerical study of brittle failure in rocks with distinct microcrack characteristics", *Int. J. Rock Mech. Mining Sci.*, **106**, 289-299. https://doi.org/10.1016/j.ijrmms.2018.04.006.

Liu, G., Cai, M. and Huang, M. (2018), "Mechanical properties of brittle rock governed by micro-geometric heterogeneity", *Comput. Geotech.*, **104**, 358-372. https://doi.org/10.1016/j.compgeo.2017.11.013.

Meng, Q.X., Wang, H.L., Xu, W.Y. and Chen, Y.L. (2019), "Numerical homogenization study on the effects of columnar jointed structure on the mechanical properties of rock mass", *Int. J. Rock Mech. Min. Sci.*, **124**. https://doi.org/10.1016/j.ijrmms.2019.104127.

Miller, D.M. (1984), "Reducing transformation bias in curve fitting", *Am. Statistician*, **38**(2), 124-126. https://doi.org/10.1080/00031305.1984.10483180.

Montgomery, D.C. (2001), "Design and analysis of experiments", John Wiley & Sons, New York.

Morris, J.P., Rubin, M.B., Block, G.I. and Bonner, M.P. (2006), "Simulations of fracture and fragmentation of geologic materials using combined FEM/DEM analysis", *Int. J. Impact Eng.*, **33**(1-12), 463-473. https://doi.org/10.1016/j.ijimpeng.2006.09.006.

Oge, I.F. (2018), "Determination of deformation modulus in a weak rock mass by using menard pressuremeter", *Int. J. Rock Mech. Min. Sci.*, **112**, 238-252. https://doi.org/10.1016/j.ijrmms.2018.10.009.

Oge, I.F. (2020), "Field evaluation of flexible support system with radial gap (FSRG) under a squeezing rock condition in a coal mine development", *Geomech. Geophys. Geo-Energ. Geo-Resour.*, **6**(3), 1-20. https://doi.org/10.1007/s40948-020-00175-9(0123456789.

Oge, I.F. (2021), "Revisiting the assessment of squeezing condition and energy absorption of flexible supports: A mine development case", *Tunn. Undergr. Sp. Tech.*, **108**, 103712. https://doi.org/10.1016/j.tust.2020.103712.

Pierce, M., Cundall, P., Potyondy, D. and Mas Ivars, D. (2007), "A synthetic rock mass model for jointed rock", *Proceedings of the 1st Canada-US Rock Mechanics Symposium - Rock Mechanics Meeting Challenges and Demands*.

Potyondy, D.O. (2015), "The bonded-particle model as a tool for rock mechanics research and application: current trends and future directions", *Geosyst. Eng.*, **18**(1), 1-28. https://doi.org/10.1080/12269328.2014.998346.

Potyondy, D.O. and Cundall, P.A. (2004), "A bonded-particle model for rock", *Int. J. Rock Mech. Min. Sci.*, **41**(8), 1329-1364. https://doi.org/10.1016 /j.ijrmms.2004.09.011.

Poulsen, B.A., Adhikary, D.P., Elmouttie, M.K. and Wilkins, A. (2015), "Convergence of synthetic rock mass modelling and the Hoek-Brown strength criterion", *Int. J. Rock Mech. Min. Sci.*, **80**, 171-180. https://doi.org/10.1016/j.ijrmms.2015.09.022.

Rasmussen, L.L., Cacciari, P.P., Futai, M.M., de Farias, M.M. and de Assis, A.P. (2019), "Efficient 3D probabilistic stability analysis of rock tunnels using a lattice model and cloud computing", *Tunn. Undergr. Sp. Tech.*, **85**, 282-293. https://doi.org/10.1016/j.tust.2018.12.022.

Sarfarazi, V., Haeri, H. and Khaloo, A. (2016), "The effect of non-persistent joints on sliding direction of rock slopes modified fish-bone model and cost-effective analyses View project The effect of non-persistent joints on sliding direction of rock slopes", *Comput. Concrete*, **17**(6), 723-737. https://doi.org/10.12989/cac.2016.17.6.723.

Scholtès, L. and Donzé, F. V. (2015), "A DEM analysis of step-path failure in jointed rock slopes", *Comptes Rendus – Mecanique*, **343**(2), 155-165. https://doi.org/10.1016/j.crme.2014.11.002

Turichshev, A. and Hadjigeorgiou, J. (2017), "Development of synthetic rock mass bonded block models to simulate the behaviour of intact veined rock",*Geotech. Geol. Eng.*, **35**(1), 313-335. https://doi.org/10.1007/s10706-016-0108-5.

Vallejos, J.A., Suzuki, K., Brzovic, A. and Ivars, D.M. (2016), "Application of Synthetic Rock Mass modeling to veined core-size samples", *Int. J. Rock Mech. Min. Sci.*, **81**, 47-61. https://doi.org/10.1016/j.ijrmms.2015.11.003.

Wang, X. and Yan, Y. (2020), "Scale effect of mechanical properties of jointed rock mass: A numerical study based on particle flow code", *Geomech. Eng.*, **21**(3), 259-268.. https://doi.org/10.12989/gae.2020.21.3.259.

Xu, Z.H., Wang, W.Y., Lin, P., Xiong, Y., Liu, Z.Y. and He, S.J. (2020), "A parameter calibration method for PFC simulation: Development and a case study of limestone", *Geomech. Eng.*, **22**(1), 97-108. https://doi.org/10.12989/gae.2020.22.1.097.

Yoon, J. (2007), "Application of experimental design and optimization to PFC model calibration in uniaxial compression simulation", *Int. J. Rock Mech. Min. Sci.*, **44**(6), 871-889. https://doi.org/10.1016/j.ijrmms.2007.01.004.

Zhou, X. and Chen, J. (2019), "Extended finite element simulation of step-path brittle failure in rock slopes with non-persistent en-echelon joints", *Eng. Geol.*, **250**, 65-88. https://doi.org/10.1016/j.enggeo.2019.01.012.

JS

List of abbreviations

UCS_m	Lattice uniaxial compressive strength
E_m	Lattice elastic modulus
T_m	Lattice tensile strength
j_m	Flat joint friction angle
$UCS(\sigma_c)$	Macro-scale uniaxial compressive strength
E	Macro-scale elastic modulus
j	Macro-scale flat joint friction angle
σ_t	Macro-scale tensile strength
ANOVA	Analysis of variance